Journal of Magnetism and Magnetic Materials 321 (2009) 2035–2047

Contents lists available at ScienceDirect

Journal of Magnetism and Magnetic Materials

journal homepage: www.elsevier.com/locate/jmmm

Current Perspectives

Recent advances in processing and applications of microwave ferrites

Vincent G. Harris [a,b,*], Anton Geiler [a,b], Yajie Chen [b], Soack Dae Yoon [b], Mingzhong Wu [c], Aria Yang [b], Zhaohui Chen [a,b], Peng He [a,b], Patanjali V. Parimi [a,b,g], Xu Zuo [d], Carl E. Patton [c], Manasori Abe [e], Olivier Acher [f], Carmine Vittoria [a,b]

[a] Center for Microwave Magnetic Materials and Integrated Circuits (CM^3IC), Northeastern University, Boston, MA 02115, USA
[b] Department of Electrical and Computer Engineering, Northeastern University, Boston, MA 02115-5000, USA
[c] Department of Physics, Colorado State University, Fort Collins, CO 80523, USA
[d] College of Information Technical Science, Nankai University, 94 Weijin Road, Tianjin 300071, China
[e] Department of Physical Electronics, Tokyo Institute of Technology, 2-12-1, O-okayama, Meguro-ku, Tokyo 152-8552, Japan
[f] CEA, Le Ripault, 37260 Monts, France
[g] Department of Physics, Northeastern University, Boston, MA 02115-5000, USA

ARTICLE INFO

Article history:
Received 21 January 2008
Received in revised form
5 December 2008
Available online 21 January 2009

Keywords:
Ferrites
Spinel
Garnet
Hexaferrite
Ferromagnetic resonance
Pulsed laser deposition
Liquid phase epitaxy
Screen printing
Negative index materials
Microwave

ABSTRACT

Next generation magnetic microwave devices will be planar, smaller, weigh less, and perform well beyond the present state-of-the-art. For this to become a reality advances in ferrite materials must first be realized. These advances include self-bias magnetization, tunability of the magnetic anisotropy, low microwave loss, and volumetric and weight reduction. To achieve these goals one must turn to novel materials processing methods. Here, we review recent advances in the processing of microwave ferrites. Attention is paid to the processing of ferrite films by pulsed laser deposition, liquid phase epitaxy, spin spray ferrite plating, screen printing, and compaction of quasi-single crystals. Conventional and novel applications of ferrite materials, including microwave non-reciprocal passive devices, microwave signal processing, negative index metamaterial-based electronics, and electromagnetic interference suppression are discussed.

1. Introduction

The value of ferrite materials have been known to ancient cultures for many centuries. As early as the 12th century the Chinese were known to use lodestone (i.e. Fe_3O_4) in compasses for navigation. However, it was not until the 1930s that modern ferrites had been studied for their magnetic, structure, and electronic properties.

Ferrite materials are insulating magnetic oxides. Unlike most materials, they possess both high permeability and moderate permittivity at frequencies from dc to the millimeter. Due to their low eddy current losses, there exist no other materials with such wide ranging value to electronic applications in terms of power generation, conditioning, and conversion. These properties also afford them unique value in microwave devices that require strong coupling to electromagnetic signals and often non-reciprocal behavior. Here, we review recent advances in ferrite processing and device development for frequencies above 1 GHz. Since, excellent reviews have been presented in previous years [1], we will focus here on advances made in these important areas since the year 2000.

The ferrite structure, be it garnet, spinel or magnetoplumbite, has as its backbone a close-packed structure of oxygen anions. Metallic cations, magnetic and nonmagnetic, reside on the interstices of the close-packed oxygen lattice. In the spinel structure (see Fig. 1a), these cations have either four- or six-fold coordination and form tetrahedra (A) and octahedra (B) sublattices that are in themselves arranged in a close-packed arrangement. (In the hexaferrites there are also cation sites that are five fold in local symmetry.)

The magnetism in these structures arises from a superexchange mechanism [2]. In the ground state superexchange is a negative exchange interaction that results in the antialignment of cation spins. This is the principle reason that ferrite magnetization is significantly reduced in comparison to the magnetism of 3d metallic alloys in which the spins are typically aligned parallel.

* Corresponding author at: Center for Microwave Magnetic Materials and Integrated Circuits (CM^3IC), Northeastern University, Boston, MA 02115, USA. Tel.: +1 617 373 7603; fax: +1 671 373 8970.
E-mail address: harris@ece.neu.edu (V.G. Harris).

0304-8853/$ - see front matter © 2009 Elsevier B.V. All rights reserved.
doi:10.1016/j.jmmm.2009.01.004

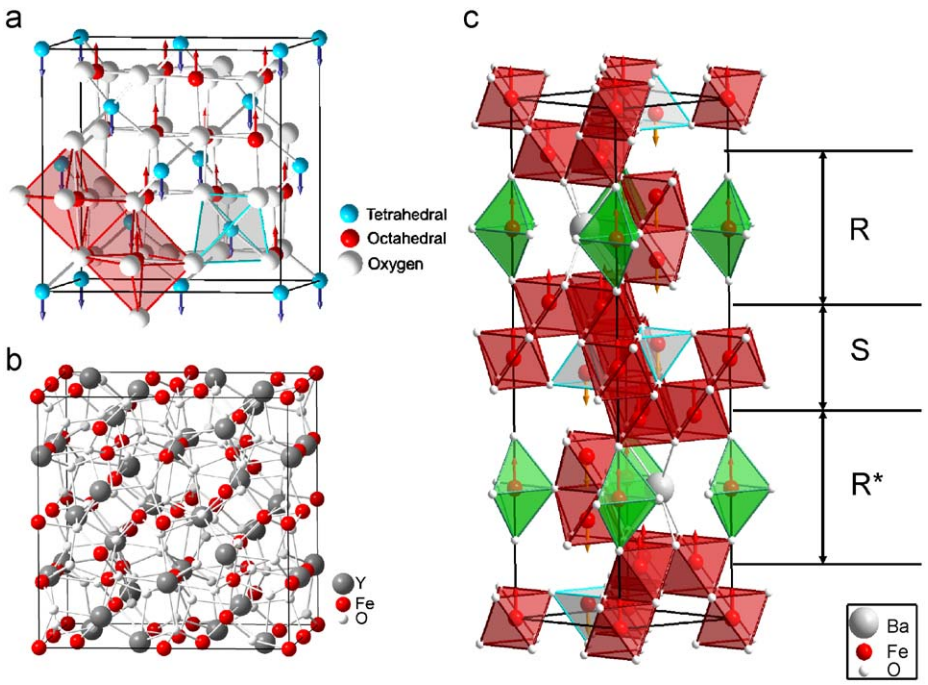

Fig. 1. Schematic representation of spinel (a) and magnetoplumbite (b) structures. The accompanying table provides information of cation site occupation and symmetry.

Because the B-site and A-site spins are antialigned, one increases the net magnetization (M) in ferrites by creating an imbalance between the sublattice magnetizations. This is typically done by substituting nonmagnetic cations for the ferrous ions. An example of this is the substitution of Zn^{2+} for A-site Fe cations. As one increases the fraction of Zn on the A-sublattice the magnetization increases at the expense of the strength of the AB exchange interaction. This strategy works to a point and then the spins on the A- and B-sublattices cant due to the reduction in the exchange constant, J_{AB}, leading to a reduction in net magnetization. For this reason, cation substitution must be carefully chosen to maximize M and maintain a strong J_{AB}.

The high-frequency permeability of ferrites, including spinels, garnets, and hexaferrites, assumes a tensor form because of the magnetically anisotropic and gyromagnetic nature of these materials. These properties stem from the fact that the precessional motion of the magnetic dipole moments is in one sense of rotation for a given magnetic bias field direction. Reversing the field direction reverses the sense of rotation. Hence, the rotational motion does not obey time reversal symmetry and gives rise to non-reciprocal behavior. The frequency of the precessional motion is proportional to the magnitude of the magnetic bias field that depends, in addition to the externally applied magnetic field, on the demagnetizing field and the magnetocrystalline anisotropy fields present in the ferrite. The interaction between a circularly polarized electromagnetic wave and the precessional motion of the dipole moments is strongest when the sense of rotation is the same in both. Since reversing the propagation direction is equivalent to reversing the sense of rotation in a circularly polarized wave, only one propagation direction will interact strongly with the ferrite. This direction-dependent nature of wave propagation in ferrite materials allows various non-reciprocal devices, such as circulators and isolators, to be developed. The strength of the interaction between the ferrite and the wave can be controlled by the external field, allowing various tunable devices, such as phase shifters and filters, to be produced. The strongest interaction occurs at ferromagnetic resonance, resulting in a strong attenuation of the wave. This property of ferrites is exploited in the design of various absorber devices.

The spinel structure is cubic and as a result the magnetocrystalline anisotropy energy is relatively small and the corresponding magnetic anisotropy fields (H_A) are typically 10s of Oe. Because the ferromagnetic resonance (FMR) frequency is strongly dependent upon H_A, the zero field FMR frequency of spinel ferrites typically falls near or below 1 GHz. Since the operating frequency is largely determined by the FMR frequency of the ferrite, this limits the frequency of devices employing spinel ferrites to C-, S-, and X-bands. In fact, for many of these applications the ferrite is biased by the field from a permanent magnet. The magnet serves to saturate the ferrite as well as shift the FMR to higher frequencies required for certain device applications. At frequencies above X-band the bias magnet is prohibitively large to make spinel devices untenable.

The garnets are another important class of ferrite material that like the spinels adopt an oxygen-closed-packed cubic structure. Garnets usually have the stoichiometry of $Y_3Fe_5O_{12}$, in which Y can be replaced by the rare-earth ions Pm, Sm, Eu, Gd, Tb, etc. Different from the spinels, which have incompletely filled cation sublattices, the garnets have all existing octahedral and tetrahedral sites occupied with metallic cations. This cation arrangement contributes to the fact that garnets have excellent structural and chemical stability. $Y_3Fe_5O_{12}$ (YIG) is one of the most important garnets for microwave applications because of its small FMR linewidth, 0.6 Oe [3], which corresponds to very low microwave loss. However, the saturation magnetization and the crystal anisotropy are rather low ($4\pi M_s = 1700$ G and $H_A = 40$ Oe, respectively) compared with other ferrite systems. As a result, YIG is usually biased by permanent magnets and used in microwave devices operating below 1–2 GHz.

At higher frequencies, ferrites with substantially higher magnetic anisotropy are required. For this, we turn to hexaferrites having the magnetoplumbite structure.

In contrast to the spinel and garnet ferrites, the magnetoplumbite structure is hexagonal in symmetry. Among the most popular of the microwave hexaferrites are those derived from the

Ba *M*-type (or Ba*M*) hexaferrite, $BaFe_{12}O_{19}$ (see Fig. 1b). Their utility stems in part from the alignment of the easy magnetic direction along the crystallographic *c*-axis and the ability to process these materials with a high degree of crystal texture. For example, the growth of Ba*M* films on appropriate lattice matched substrates lead to crystal texture and subsequent to perpendicular magnetic anisotropy: a requirement for conventional circulator devices.

During the past decade, research on *Y*-, *U*-, *W*-, *X*- and *Z*-type hexagonal ferrites have resulted in properties useful for many microwave applications. For example, unlike the *M*-type ferrites, *Z*-type ferrites have their magnetic easy axis aligned along the *a*–*b* plane. This is of particular value for conventional phase shifters. This research is not discussed in great detail in this review due to space constraints. We do discuss at length the properties of *M*-type ferrites with the implication that materials processing and device refinement are generally transferable to other ferrite systems.

The *M*-type hexaferrite consists of spinel blocks (*S*) that are rotated 180° with respect to one another and separated by an atomic plane containing the Ba atoms (*R* blocks). This plane of atoms breaks the crystal symmetry resulting in the hexagonal structure and large magnetocrystalline anisotropy energy. Such a high anisotropy arises also from dipole–dipole interactions and single ion anisotropy. Remarkably, the magnetic anisotropy field in this ferrite is ~17,500 Oe or 1000 times greater than some cubic spinels [4,5]. The large H_A places the zero field FMR frequency near 36 GHz. Thus, while an externally applied magnetic field is still necessary to saturate the ferrite, due to the large H_A the magnitude of the applied field required to shift FMR to sufficiently high frequency is substantially lower. As such, devices based upon this ferrite can operate at frequencies as high as Ka-band (for below resonance operation). Furthermore, textured polycrystalline hexaferrites can be produced with permanent magnet properties, such that they remain in a magnetized state in the absence of an externally applied magnetic field. In this condition, referred to as self-bias, the high internal bias field required for device operation at high frequencies is achieved without external biasing magnets.

The Ba*M* system is remarkably versatile in that substitutions for the Fe cation can drastically reduce or increase the H_A. For example, the substitution of Sc or In for Fe reduces the anisotropy field allowing for applications from C, X, Ku, K, to Ka bands [6]. Substitution of Al and Ga lead to increases in H_A and device applications at frequencies up to and including U, E, and W bands [7]. In essence, the Ba*M* hexaferrites and its substitutional systems allow for device applications from 1 to 100 GHz. Additionally, the unique high crystalline anisotropy field of Ba*M* allows the possibilities to retain high remnant magnetization when the external applied field is removed. Usually, the ferrite-hosted microwave transceivers requires the use of permanent magnets to bias the magnetic material for operation at certain frequencies. Those magnets hinder efforts to reduce the size and weight of the resulting devices. With the possibility of obtaining high effective internal fields, the need for external permanent magnets is eliminated. The realization of the self-biased Ba*M* material will have a wide ranging impact on the development of planar microwave passives leading ultimately towards MMIC integration.

In order to meet the needs of next generation microwave device technologies, ferrite materials must be made to have specialized properties. For passive devices such as circulators, isolators, phase shifters, delay lines, etc., these include control of the amplitude and direction of magnetic anisotropy fields, low FMR linewidths, self-bias properties, and thicknesses in the 10s to 100s of microns. A paradox that we face in refinement of these materials is that many of these properties are optimized in single crystals (e.g. anisotropy fields and low FMR linewidths), whereas other properties (e.g. self-bias or high remanent magnetization values) typically require high coercive fields that are often inherent in polycrystalline materials. This dichotomy requires compromise in the choice of materials processing methods. The fact that these materials may be 100s of microns thick further limits the choice of processing methods. In contrast, for the case of electromagnetic interference (EMI) suppression, material properties for these applications require high permeability but also high losses that readily allow for the absorption of electromagnetic signals. It is also desirable to either deposit magnetic materials directly over circuit board elements or create flexible sheets that can be pasted over the radiating elements. These processing methods have until recently proven elusive.

In the next sections, we will discuss recent trends in processing of ferrite materials for microwave device applications.

2. Advances in microwave ferrite processing

2.1. Thin film processing using PLD and ATLAD

Pulsed laser deposition (PLD) is a well-established method for growing ferrite films. In conventional PLD (Fig. 2a and b), laser pulses from a high energy laser (e.g. an excimer) ablate a homogeneous target forming a molecular flux (or plume). The substrate intercepts the plume allowing for film growth on selected, often lattice-matched, substrates (Fig. 2a). PLD has been used in the deposition of garnet, spinel, and hexaferrite ferrites. The deposition of epitaxial yttrium iron garnet films by PLD was first demonstrated by Dorsey et al. in 1993 [8,9]. Films with a thickness of about 1 μm were deposited on (111) gadolinium gallium garnet (GGG) substrates. Narrow FMR linewidths of <1 Oe were observed in the films deposited under low oxygen pressure (<250 mT) and high substrate temperature (>800 °C). Thin films of $Bi_3Fe_5O_{12}$ (BIG), $Eu_1Bi_2Fe_5O_{19}$ (EBIG) as well as YIG/BIG and YIG/EBIG heterostructures, have been investigated by Simion et al. [10]. Increased saturation magnetization was observed in the YIG/BIG heterostructures compared to that of single layer films [11]. Thick (~50 μm) epitaxial YIG films with a linewidth of 5.7 Oe were deposited on (111) GGG substrates at a high rate by Buhay et al. [12]. In the same paper, the deposition of polycrystalline thick (50–100 μm) films on gold-coated (100) Si wafers followed by rapid thermal annealing was reported. More recently, the magneto-optical properties of Ce [13,14] and Bi [15,16] substituted YIG films and YIG/GGG superlattices [17] grown by PLD on (111) GGG substrates have been investigated.

Growth of ferrite films using PLD was first proposed by Vittoria in 1991 [18], inspired by the PLD growth of high-T_c superconducting films. The first Ba*M* hexaferrite films grown by PLD were reported by Dorsey et al. in 1992 [19]. In the years following this work many researchers have applied PLD to ferrite film synthesis. Among the highest quality Ba*M* films made today are those by Song et al. [20] who achieved perpendicular magnetic anisotropy (Fig. 3a) and an FMR linewidth of ~16 Oe at 60.3 GHz (Fig. 3b).

The above mentioned studies had strived to align the crystallographic *c*-axis and the magnetic easy axis perpendicular to the film plane. In-plane orientation of Ba*M* films can be achieved by using suitable substrates that are chosen for their lattice matching (e.g. *a*- or *m*-cut sapphire). Alternatively, Y- or Z-type hexaferrites can be grown having the magnetic polarization in the basal plane. Welch et al. reported in 1995 that the *c*-axis of Ba*M* films deposited on the in-plane substrate was randomly distributed in the film plane [21]. Yoon et al. subsequently reported in 2003 that the *c*-axis of the Sc*M* (scandium-doped Ba*M*) films deposited

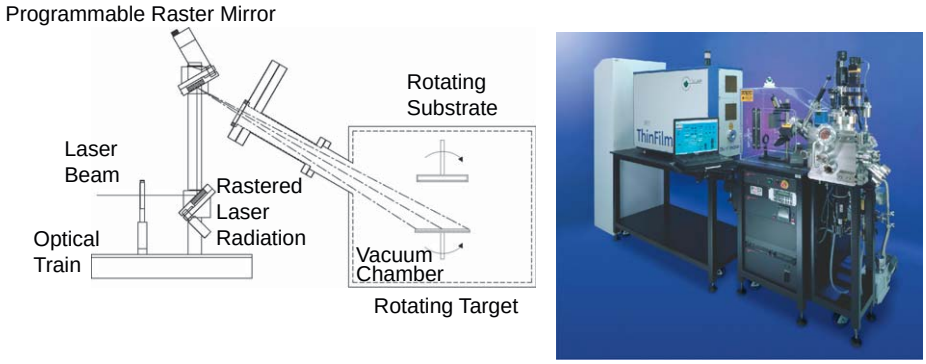

Fig. 2. (a) Schematic and (b) photograph of a typical pulsed laser deposition system. (Courtesy of PVD Inc, Wilmington, MA 01887; http://www.pvdproducts.com/default.aspx)

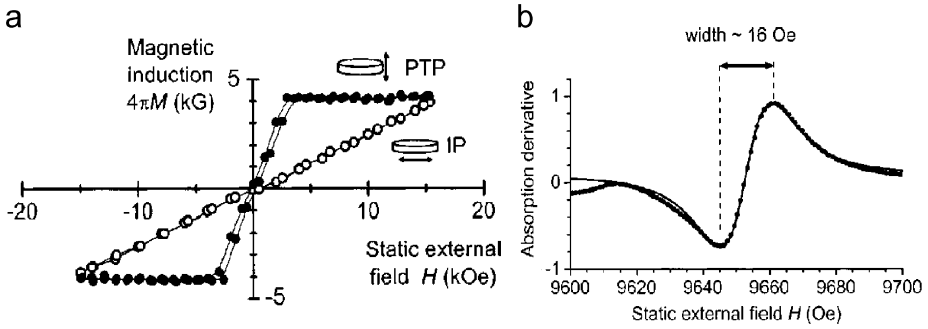

Fig. 3. (a) Magnetic induction $4\pi M$ vs. static external magnetic field H for a PLD grown 0.85 μm thick BaM film. The field was applied perpendicular to plane or in-plane. The points show the data and the lines show spline fits as a guide to the eye. (b) Expanded view of the absorption derivative vs. static external field H at 60.3 GHz for the main ferromagnetic resonance mode. The closed circles show the data. The solid line shows a fit to the data based on a Lorentzian absorption response with resonance field of 9653 Oe, half power linewidth of 27 Oe, and 11% baseline shift. (Ref. [20]. Reproduced with the permission of the authors).

on a-cut sapphire aligned in the film plane parallel to the c-axis of the substrate [22].

A long sought goal of the ferrite community has been the integration of ferrite-based microwave passive devices with semiconductor electronics. This requires the growth of ferrites on semiconductor substrates. Oriented hexaferrite films deposited on semiconductor substrates are made difficult by the high temperatures required to grow a ferrite having low microwave loss. Further difficulties arise from the formation of native oxides on the substrate surface leading to a loss of epitaxy when growing the ferrite. Liu et al. reported in 2005 the growth of oriented BaM films on silicon substrates with an MgO buffer layer [23]. Chen et al. reported in 2006 the growth of oriented BaM thin films on 6H–SiC substrates with and without a MgO buffer layer [24,25]. The latter studies included the growth of BaM having perpendicular magnetic anisotropy and an FMR linewidth (peak-to-peak in the power derivative) of less than 100 Oe at 53 GHz [136].

Besides BaM, many hexaferrite materials have been deposited by PLD. Other M-type hexaferrites, strontium and lead hexaferrites (SrM and PbM), have been studied as films [26,27]. Scandium-doped BaM films were deposited to control the magnetic anisotropy, [28] whereas cobalt and titanium co-doped BaM and aluminum-doped SrM films were deposited for the optimization of the magneto-optical properties [29,30].

Growth of spinel ferrites using PLD was first realized by Tanaka et al. in 1991. In this work, nickel zinc ferrite ($Ni_xZn_{1-x}Fe_2O_4$) polycrystalline films were deposited on glass substrates [31]. Johnson et al. reported in 1999 the growth of nickel ferrite ($NiFe_2O_4$) on $c-$cut sapphire substrates using both PLD and ATLAD [32]. Chinnasamy et al. reported in 2007 the PLD growth of Ni-ferrite films on MgO (111) substrates. In this study, as in others, post-annealing was found to enhance the magnetic properties of the films, including increasing the magnetization and reducing the FMR linewidth [33].

Balestrino et al. reported in 1995 the PLD growth of lithium ferrite ($Li_{0.5}Fe_{2.5}O_4$) and Mn-and Zn-doped lithium ferrite films [34]. Cillessen et al. reported in 1996 the epitaxial growth of MnZn-ferrite films on $SrTiO_3$ with and without $BaZrO_3$ buffer layers [35].

Guyot et al. reported in 1996 the growth of cobalt ferrite films [36]. In 2004, Terzzoli et al. reported the growth of Co-ferrite films on Si (1 0 0) substrates with a strong (1 1 1) crystal texture in spite of the formation of a native oxide layer at the substrate surface. Yang et al. illustrated enhanced magnetization in PLD Cu-ferrite films as a function of working gas pressure-induced cation disorder [37].

A variant to conventional PLD involves the sequential ablation of atomic layers from multiple targets. This allows one to control cation distribution in the unit cell leading to the stabilization of ferrites having far from equilibrium structures. This technique has been referred to as alternating target laser ablation deposition or ATLAD. In recent years, ATLAD has been used by Zuo et al. [38], and Yang et al. [39], to realize far from equilibrium cation distributions within the spinel lattice for Mn- and Cu-ferrite film systems, respectively. In the case of Mn-ferrite films, low oxygen pressure processing lead to a low cation inversion and large single ion anisotropy, increasing H_A from ~20 to >1000 Oe. In contrast, at high pressures the cation inversion increases, distorting the cubic structure, breaking the crystal symmetry, and stabilizing a perpendicular magnetic anisotropy field of ~1000 Oe. This affords these films unique potential for microwave applications at higher frequencies than normally associated with spinel ferrites. In the

Cu-ferrite film system, Yang et al. was able to redistribute the Cu ions from predominantly octahedral sites (~85%) to predominantly tetrahedral sites (~60%). This created an imbalance of spins between the A- and B-sublattices resulting in a magnetization increase of 65% (see Fig. 4a–c). Such a significant increase was predicted by Zuo et al. from first principles band structure calculations [40].

Recent studies by Geiler et al. [138] demonstrated the construction of unique ATLAD-deposited Mn-doped BaM films in which the Mn cation site occupancy was simulated, controlled and confirmed. This work was made possible in part by Yang et al. [137] who first applied diffraction fine structure spectroscopy (DAFS) to ferrites allowing for the determination of element-specific and site-specific cation occupancy and valency that allow improved control over cation engineering in ferrites include the application of diffraction fine structure spectroscopy (DAFS) to measure the element-specific, site-specific cation distribution in spinels [137], and the demonstration by Geiler et al. to design, fabricate, and verify cation placement in Mn-substituted Ba*M* films [138].

Limitations of PLD and ATLAD ferrite film fabrication include film thickness, typically $<2\,\mu m$, and high-temperature processing, typically $>700\,^{\circ}C$. At these thicknesses the films are not well-suited for device applications, while at these high temperatures the process is incompatible with semiconductor device fabrication. As a result, PLD remains a valuable research tool but does not adequately address the materials needs of the microwave device community. During the last decade, Abe and coworkers have developed a wet chemistry deposition technique, spin spray ferrite plating, which allows low-temperature processing of thicker ferrite films. We next discuss the advantages and disadvantages of this technique.

2.2. Spin spray ferrite plating

In spin spray plating (SSP) the nucleation and growth of a solid phase film is facilitated by hydrolysis without pyrolysis. Abe et al. first began developing SSP during the mid 1980s as a means of processing ferrite films at low temperatures [41]. The advantages of SSP include rapid growth rates, thick dense films, and the low-temperature processing on a myriad of substrate materials that range from plastics to ceramics. The technique is pictured in Fig. 5a and b and involves the spraying of metal acid solutions (commonly metal chloride solutions) and oxidizing agents (commonly sodium nitrite solutions) via nebulizers onto rotating substrate materials held at temperatures ranging from room

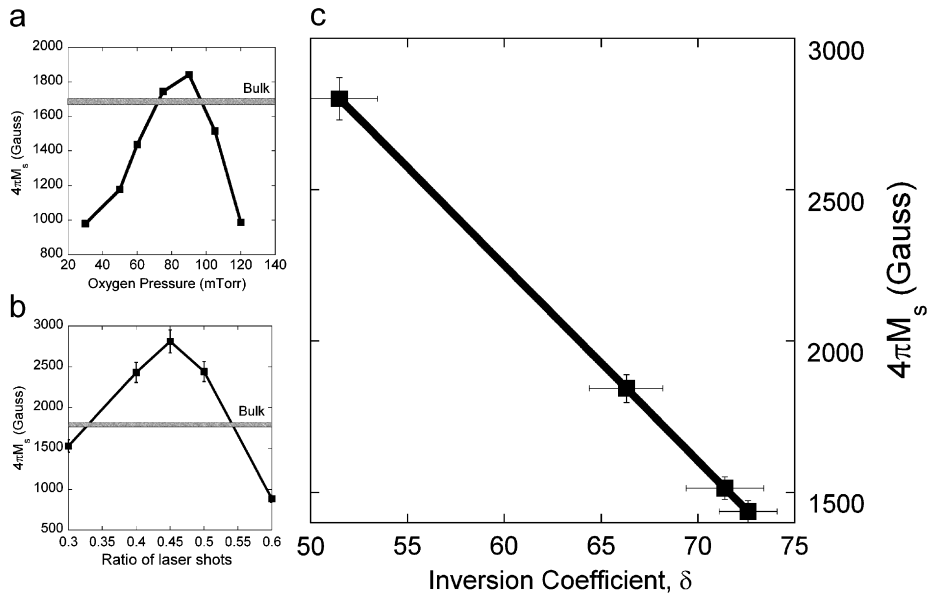

Fig. 4. The saturation magnetization is plotted as a function of (a) oxygen pressure used during deposition, (b) the ratio of laser shots incident on CuO and Fe_2O_3 targets, and (c) inversion parameter (i.e. the percentage of Cu residing at B-sites). (Ref. [39]. Reproduced with the permission of the authors).

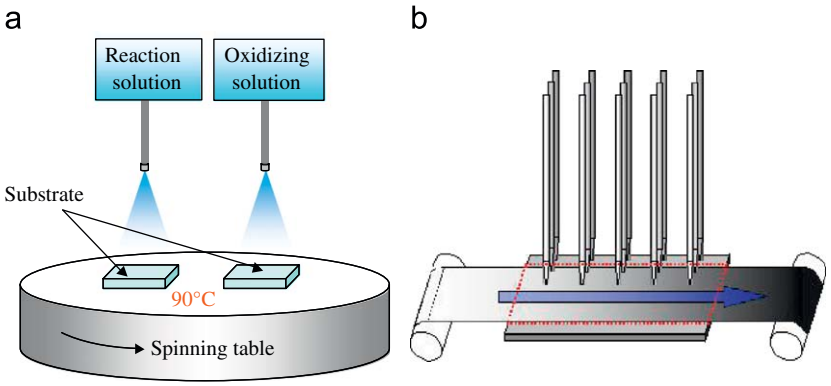

Fig. 5. (a) Schematic of a conventional spin spray apparatus, a chemical method for the preparation of ferrite films from aqueous solutions. (b) A variant of SSP that allows for the ferrite plating of rolls of polymer materials.

temperature to 90 °C. By ferrite plating one can prepare polycrystalline films having the spinel structure ($(M,Fe)_3O_4$, M = Fe, Co, Ni, Zn, Mn, etc.) directly from an aqueous solution. This technique has recently been extended to the deposition of ferrites onto rolls of plastic sheet [42].

Requiring no post-deposition heat treatments, SSP has made available depositing ferrite films on such non-heat-resistant materials as semiconductor substrates [43] and polymer sheets [44] for EMI suppression and other purposes.

The Abe research group has developed NiZn-ferrite noise suppressors, which absorb electromagnetic currents by magnetic losses before they radiate as noise, for applications in the low microwave bands. In one approach, ferrite films are deposited onto polyimide sheets, which are cut and pasted onto noise sources. A second approach, NiZn-ferrite films are deposited directly onto printed circuit boards, covering potential noise sources such as ICs and conducting wires [45].

SSP NiZn-ferrite films, 3 μm thick, have been shown to suppress GHz noise more effectively than commercialized noise suppressors consisting of composite sheets in which fine magnetic metal flakes are embedded in polymer sheets. The sheet type noise suppressors, made by the roll spray ferrite plating process (Fig. 5b), have attractive properties, including surface resistivities higher than $1\times10^5\,\Omega/cm^2$, stability to temperatures greater than 260 °C (i.e. the lead-free soldering temperature [42]), and the ability to withstand the standard bend test (JIS C5016): no peel-off occurred after one million cycles of bending at a 3 mm radius of curvature [46]. Spin sprayed NiZnCo ferrite films have been shown to have very high natural resonance frequencies from 3 to 5 GHz and values of μ' from 5 to 8 up to a few GHz. These films are promising as magnetic field shielding to improve, for example, the sensitivity of 900 MHz RFID tags for next generation applications [47].

Even with the thicker films one obtains in using SSP, these samples still fall short of the needs for many microwave device applications. The FMR linewidths of SSP films are higher than those processed by PLD with the losses attributed to contaminants from the chemical processing. Liquid phase epitaxy (LPE) is a technique that has been shown to provide both thick films and high crystal quality. We next examine the magnetic and structural properties of LPE grown of ferrites.

2.3. Liquid phase epitaxy

In liquid phase epitaxy, oxide compounds such as ferrites are mixed and dissolved in solvents or fluxes (i.e. common fluxes include boron oxide (B_2O_3), barium oxide (BaO) and B_2O_3, lead oxide (PbO), or a mixture of B_2O_3/PbO). In general, the composition of the flux mixtures is chosen so that the melt temperature for most ferrites is less than 1000 °C. The substrate acts as a seed onto which the ferrite film grows when the melt temperature is lowered below the liquidus. Appropriate lattice matching between film and substrate is considered to minimize strain-induced crystal defects.

LPE was first employed to produce high-quality yttrium iron garnet (YIG: $Y_3Fe_5O_{12}$) films by Linares in 1968 [48]. LPE grown garnets continue to receive a great deal of attention for high-frequency applications such as microwave and millimeter wave devices and optical Faraday isolators [49–53]. Growth rates in LPE can be greater than 50 μm/h leading to film thicknesses of 200 μm or more [54]. This is a definite advantage over other deposition techniques including physical or chemical vapor deposition methods. In all film deposition processing methods that aim to maintain epitaxy a common difficulty is the lattice mismatch between ferrites and crystal substrates. A favored substrate for the deposition of garnets, gadolinium gallium garnet (GGG) has the garnet crystal structure with a close match to the thermal expansion coefficient of YIG, in addition to a lattice mismatch of only 0.06% [49,54]. Further, GGG is among the highest quality, commercially available, crystal substrates having wafer diameters up to 3 in. Although the lattice mismatch is exceedingly small compared to the mismatches of many epitaxial semiconductor materials or oxides (i.e. spinels and hexaferrites), these mismatches can have deleterious effects upon film structure and properties. However, the growth of YIG by LPE on double-sided GGG provides a cancellation of the in-plane tensile stress that allow for the growth of film to thicknesses in excess of 200 μm. These films have been measured to have FMR linewidths of less than 1 Oe at ~9 GHz [54]. The success of LPE in the growth of high-quality YIG films lead to similar LPE processing of spinel ferrite films. A number of spinel ferrites have been grown by LPE [55–59], but crystal quality and thickness of the films has yet to reach the level of the garnets. This may be due to crystal defects resulting from mismatches in substrate lattice parameters and/or thermal expansion coefficients. As a result, it has been difficult to consistently deposit high quality and reasonably thick spinel ferrite films, such as $LiFe_2O_4$, having linewidths consistently below 20 Oe [58]. Notwithstanding these challenges, the smallest recorded FMR linewidth for LPE grown Li-ferrite is below 10 Oe [74].

LPE grown hexagonal ferrites, especially barium hexaferrite, have received great attention [60–65]. The smallest linewidths obtained for LPE grown epitaxial barium hexaferrite on single crystal hexagallate ($SrGa_{12}O_{19}$) substrates were ~45 Oe at 60 GHz [66]. These values should be compared with $\Delta H<10$ Oe for the best barium hexaferrite single crystal sphere [54,67,68] and a value of ~10 Oe predicted for Mn-doped hexagonal ferrite [69,70]. Recently, hexagonal ferrite films having the *c*-axis perpendicular to the substrate plane have been grown by LPE on PLD grown seed layers on commercially available substrates [71–75]. The best ΔH value, 28 Oe, was measured from a 45 μm film grown on double-sided (111) MgO [72]. Alternatively, a 200 μm Ba*M* film with the *c*-axis aligned along the in-plane direction, grown on double-sided *m*-plane Al_2O_3 [73–75], had a ΔH of 70 Oe at 60 GHz.

The LPE technique has clear advantages over other physical and chemical deposition techniques, producing very thick films (>200 μm) having high crystal quality that in some cases approaches that of single crystals. These films are very well-suited for microwave and millimeter wave devices that require low losses. However, they continue to require biasing magnets to saturate the film during operation, thus adding size, weight, and assembly cost to devices and systems. We next examine a technique that provide film thicknesses in the 100s of microns but has traditionally offered poor crystalline quality and high microwave losses.

2.4. Screen printing

In general, large area thick films can be achieved by physical processes such as tape casting, screen printing, etc. Due to simplicity and cost-effectiveness, the screen printing technique has been extensively used in mass production of multilayer chip inductors, transformers, ceramic thick film circuits, and magnetic sensors and actuators [76–78].

It is anticipated that the next generation of magnetic microwave devices will be planar, self-biased and low-loss. Additionally, these materials must be realized through cost-effective processing at industrial scales. Self-biasing is an important property that eliminates the need for the permanent bias magnet and reduces the size, weight, and cost of microwave devices [79]. In addition to high remanent magnetization and low microwave losses, thickness of the ferrite films from 100 to 500 μm may be required.

Yuan et al. [80] reported screen-printed Sr*M* films on alumina substrates by hydrothermal synthesis. The work detailed

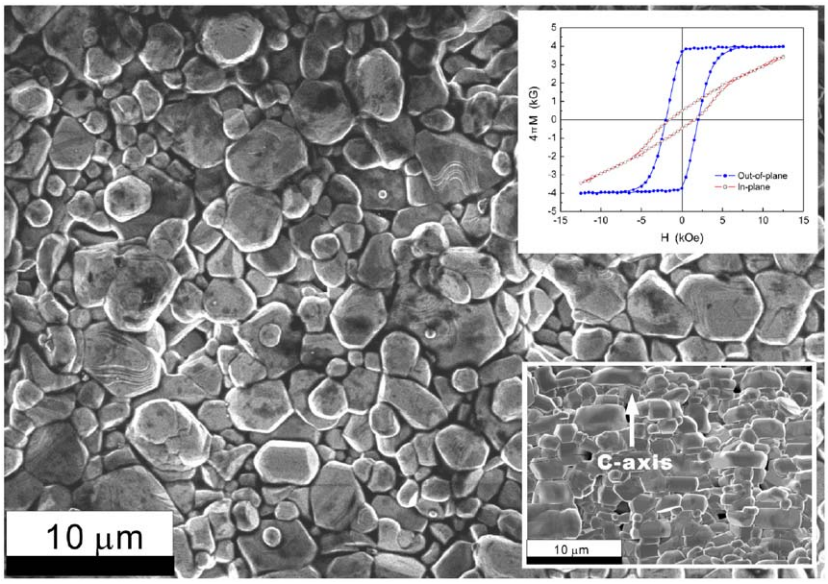

Fig. 6. Scanning electron microscopy image of the surface of an optimally prepared screen printed Ba*M* film. The lower inset is an SEM image of the films cross section showing the stacking of hexagonal platelet grains. The upper inset plot is hysteresis loops collected with the applied magnetic field aligned parallel (hollow symbols) and perpendicular (solid symbols) to the plane of the film. The hysteresis loops indicate both perpendicular magnetic anisotropy and self-bias properties. (Ref. [83]. Reproduced with permission of the authors).

influences of original powders and sintering processes on static magnetic properties. Because of thicknesses ranging from 8 to 15 μm and the low value of *M* vs. *H* loop squareness (M_r/M_s), 77%, these films failed to meet the requirements of self-biased microwave electronic devices.

Chen et al. [81,82] demonstrated the processing of Ba*M* thick films (100–500 μm), which were prepared by screen printing followed by sintering heat treatments. Structural, magnetic and microwave measurements confirmed that the polycrystalline thick films were suitable for applications in self-biased microwave devices in that they exhibited a large remanence ($4\pi M_r = 3800$ G), high hysteresis loop squareness, $M_r/M_s = 0.96$, and relatively low microwave loss (derivative linewidths of ~310 Oe at 55.6 GHz) [83]. Among those mechanisms contributing to the losses, an extrinsic linewidth broadening ($\Delta H_{ex} = 274$ Oe) was clearly dominant. This linewidth contribution arose predominantly from pores and the misalignment of grains. Subsequently, a narrower linewidth, $\Delta H = 212$ Oe at 53.5 GHz, was measured for screen-printed thick films by including a hot-press sintering step [84]. Fig. 6 shows a scanning electron microscopy (SEM) image with the cross-section as the inset of the Ba*M* film having 250 μm thickness. The second inset is a plot of hysteresis loops illustrating the high remanent magnetization providing self-bias properties. Although the film still contains pores and misaligned grains, the results have demonstrated that the screen printing technique is capable of processing thick, self-biased, and low-loss Ba*M* films in a scalable and cost-effective manner; an integral step in the processing of planar microwave magnetic devices. Paradoxically, the existence of pores plays an important role in providing the required coercivity to maintain a high remanent magnetization. The removal of the pores leads to improved linewidth at the expense of self bias properties.

2.5. Highly oriented and quasi-single crystal compacts

For devices which operate at $f < 40$ GHz, Sc- or In-doped Ba*M* or Sr*M* hexaferrites are primarily considered due to their low FMR frequencies. For example, $BaFe_{11}ScO_{19}$ ferrites, prepared by conventional ceramic processing, demonstrated a magnetization squareness of 83% and anisotropy field of less than 10 kOe. Unfortunately, the X-band FMR derivative linewidths were measured to be more than 800 Oe [85].

Most recently, low microwave losses and high squareness of the hexagonal Sc-doped Ba ferrites, also having low magneto-crystalline anisotropy fields ($H_A = 4$–10 kOe), have been successfully achieved. Chen et al. made use of a polymer network-assisted alignment processing (PNAAP) technique to effectively align hexaferrite particles in high magnetic fields to realize a highly dense oriented Sc-doped Ba ferrite compact [86]. A two-step temperature treatment of the resulting compact lead to FMR linewidths of ~500 Oe at X- and Ka-band and high magnetization squareness, M_r/M_s,~92%. These materials have unique potential for use in self-biased microwave and millimeter devices at frequencies from 1 to 40 GHz.

A quasi-single crystal (QSC) $BaFe_{12}O_{19}$ ferrite has also been realized and attracted interest from the microwave engineering community [87]. The material was fabricated by a single solid-state reaction technique that includes the alignment of the ferrite seed crystals. This technique is cost-effective in producing future microwave devices compared with those that employ Ba*M* single crystals. The QSC ferrite bulk samples show similar static magnetic properties to those of single crystals. However, its FMR linewidths are ~300 Oe at U-band frequencies, broader than Ba ferrite single crystals, <100 Oe. Nevertheless, a 300 Oe linewidth is believed to be acceptable for many practical device applications.

3. Next generation microwave and millimeter wave devices

The above section reviewed some of the processing methods and properties of ferrite films and compacts. This section will review the applications of ferrites in microwave and millimeter wave devices. In particular, we focus on recent developments in (i) microwave circulators, (ii) microwave signal processing, (iii) electromagnetic noise suppression, and (iv) new devices based upon negative index metamaterials incorporating ferrites.

The initial work in ferrites as microwave materials was motivated by the need for magnetic insulators in high-frequency inductor cores. Carried out by Snoek [88,89] and collaborators in 1930s and 1940s, this research focused on the development of high permeability materials without the losses associated with eddy currents. Seeking to take advantage of the dielectric properties of this family of ferromagnetic oxides, as early as mid 1950s a wide variety of microwave ferrite devices, including spinel ferrite-based circulators, isolators, phase shifters, directional couplers, power limiters, etc. were reported [90]. It was well understood in the early stages of high-frequency ferrite device development that the magnetic loss and the performance of such devices were highly dependent on the FMR linewidth, a measure of damping in the spin relaxation process [91]. The introduction of a new family of rare-earth ferrites of the garnet crystal structure in 1956 was, therefore, very significant, since this class of materials possesses narrower FMR linewidths than any spinel ferrite [92–94]. Ferrites of hexagonal crystal structure were identified as candidates for applications at high frequencies due to the high uniaxial magnetic anisotropy field that can be utilized to bias these materials in the microwave and millimeter-wave regions [95].

3.1. Microwave non-reciprocal passive components: the circulator

The circulator is one of the most frequently utilized ferrite devices in modern microwave systems. It is a passive non-reciprocal multi-port device that exhibits low insertion loss in the forward direction of wave propagation and high insertion loss in the reverse direction. It is used to control the power flow and to isolate various components in high-frequency systems. For example, *Y*-junction circulators, depicted schematically in stripline configuration in Fig. 7(a), are often utilized in multiple transmit–receive (*T*/*R*) modules that shape and steer the beam of phased array radar systems [96]. *T*/*R* modules, the simplified block diagram of which is shown in Fig. 7(c), combine monolithic microwave-integrated circuits (MMIC) and digital circuitry implemented on high-frequency semiconductor substrates, such as gallium–arsenide and gallium nitride, to produce high-performance, high-efficiency, low-weight, low-cost, and small-size modules [97].

First waveguide *Y*-junction circulators were reported in the late 1950s [98,99] with stripline designs following soon thereafter [100]. The first monolithic microstrip circulator on a garnet substrate was introduced in 1965 [101]. The theory of stripline *Y*-junction circulators was developed by Bosma [102,103] in 1962, and Fay and Comstock [104] in 1965. These theories explained the non-reciprocal behavior of the ferrite-loaded stripline *Y*-junction in terms of the splitting of the counter-rotating dielectric resonance modes in the ferrite material due to the off-diagonal elements of the permeability tensor proposed by Polder [105,106]. Typical electric field configuration in the ferrite-loaded stripline *Y*-junction, computed by finite element methods, is shown in Fig. 7(b). The conditions necessary for circulation over a full octave bandwidth in microstrip devices were demonstrated by Wu and Rosenbaum [107] in 1974. The extensive literature on circulator theory and design is reviewed in the annotated bibliography by Knerr [108] and in books by Von Aulock and Fay [109] and Helszajn [110].

The need to miniaturize circulator devices, to facilitate broader integration with monolithic microwave circuits and to extend the applicable frequency range into the millimeter-wave regime, motivated studies utilizing the unique properties of hexagonal ferrites. As mentioned earlier, textured polycrystalline hexagonal ferrites, such as barium and strontium hexaferrite, can be produced with permanent magnet properties such that they will remain in a stable magnetized state in the absence of an external bias field (i.e. self-biased). High uniaxial magnetic anisotropy

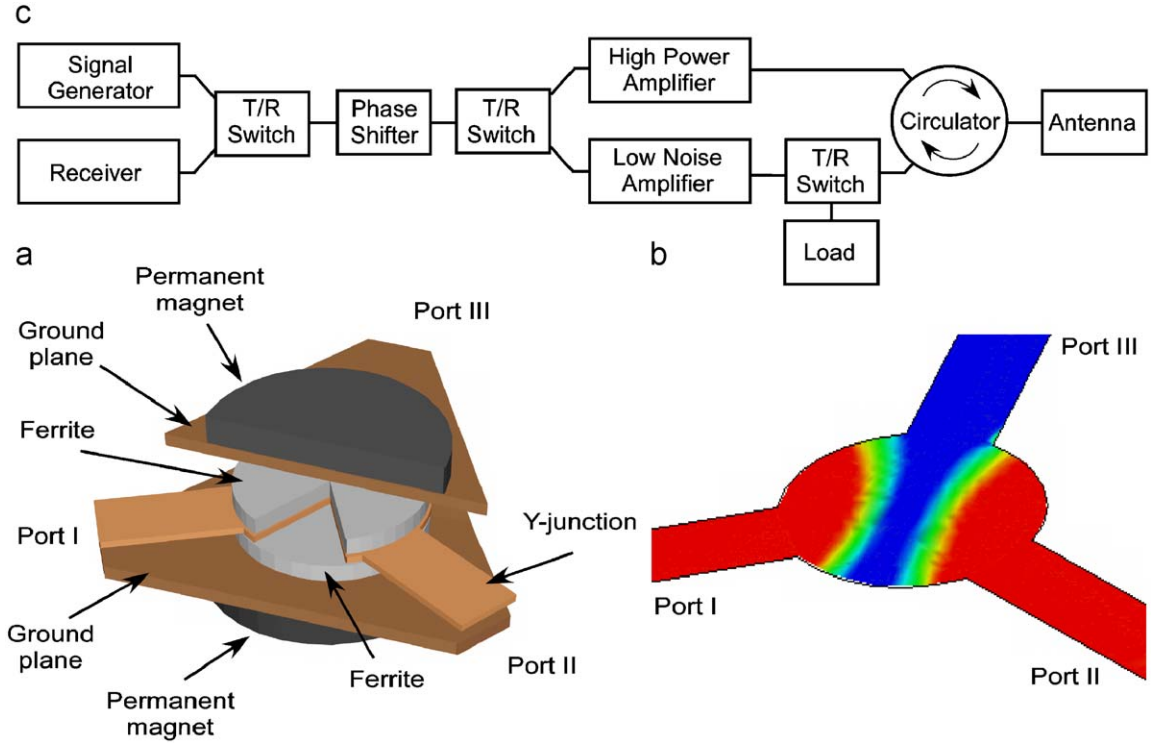

Fig. 7. (a) Components of a stripline *Y*-junction circulator. Permanent magnets provide the magnetic field necessary to bias the ferrite-loaded junction. (b) Magnitude of the electric field in the stripline *Y*-junction circulator calculated by finite element methods. Low insertion loss in the forward direction of propagation (port I–port II) and high isolation in the reverse direction (port I–III) are observed. (c) Simplified block diagram of a *T*/*R* module. Switches and a circulator are utilized to guide the high-power transmitted signal to the antenna in the transmit mode and to guide the low-power signal from the antenna to the low-noise amplifier and the receiver in the receive mode. The circulator also serves to protect the high-power amplifier by dissipating the power reflected from the radiating antenna in the load.

fields in these materials (up to 20 kOe) can be utilized to decrease or eliminate the external biasing field requirement according to Kittel's [111] resonance equation that incorporates both dipolar and magnetocrystalline anisotropy interactions.

Polycrystalline-textured strontium hexaferrite (Sr*M*) with a remnant magnetization of approximately 3.5 kG, uniaxial anisotropy field of 18.4 kOe, and FMR linewidth of approximately 2 kOe was utilized to develop a self-biased waveguide junction circulator operating at 73.5 GHz by Akaiwa and Okazaki in 1974 [112]. The reported insertion loss at center frequency was 1.1 dB with isolation exceeding 20 dB over a 2.4 GHz bandwidth. In 1989, polycrystalline Sr*M* was utilized by Weiss et al. to develop a self-biased waveguide circulator operating at 30.7 GHz with an insertion loss of less than 1 dB and isolation of more than 20 dB over a 1% bandwidth [113]. In the same paper, a self-biased microstrip design was also reported. Insertion loss of less than 2 dB and isolation over 20 dB were observed in a band of 5%. In 1992, a textured barium/strontium ferrite with remanent magnetization of 3.5 kG and uniaxial anisotropy field of 21 kOe was utilized by Zeina et al. to design microstrip and stripline circulators operating at 37 and 32 GHz, respectively [114]. In 2001, an integrated self-biased microstrip circulator was fabricated by Oliver et al. through bonding of textured Sr*M* platelets to silicon substrates in a low-temperature process compatible with semiconductor fabrication requirements [115]. Insertion loss of 2.8 dB and isolation of 33 dB were measured at 28.9 GHz with a 20 dB bandwidth of 1%. Circulator designs utilizing single crystal platelets of Sc*M* with saturation magnetization of 3.9 kG, uniaxial anisotropy field of 8.7 kOe and linewidth of 100 Oe embedded into glass-microwave integrated circuit wafers resulted in operation at 22.2 GHz with a minimum insertion loss of 2 dB and isolation of 21 dB. This performance was obtained by Shi et al. with ferrite platelets partially saturated by an externally applied magnetic field of 2 kOe (55% saturation) [116].

Another important circulator design that has the potential for monolithic microwave circuit integration and self-biased operation is the ferrite-coupled-line (FCL) circulator. Discovered experimentally in 1980s, in contrast to *Y*-junction circulators, FCL circulators utilize longitudinally magnetized ferrite materials to couple the modes between closely spaced wave guiding lines [117]. The non-reciprocity of ferrite-coupled waveguides was explained in terms of coupled mode theory by a number of researchers [118–120]. FCL circulators have the potential advantages of broad bandwidths, planar layouts, and smaller biasing fields [121,122]. Self-biased designs utilizing hexagonal ferrites have also been reported [123]. Due in part to a lower demagnetizing factor associated with a longitudinally magnetized film, self-biased epitaxial hexaferrite films are easier to produce at thicknesses necessary for device fabrication [73]. Therefore, while most self-biased *Y*-junction circulator designs fall in the quasi-monolithic category, where the ferrite is bonded or embedded in the dielectric or semiconductor substrate by various means, self-biased FCL circulators have the potential for true monolithic integration where the ferrite film is deposited and metallized with proper circuitry during one of the steps of the device fabrication process. There is no doubt that circulator designs, briefly described in this paper, as well as other high-frequency ferrite devices, will continue to benefit from further advances in ferrite materials and their integration with semiconductor substrates. Low-loss textured polycrystalline hexagonal ferrites may play an important role in device miniaturization due to their potential for self-biased operation leading to volumetric and weight reduction.

3.2. Applications of ferrite films in microwave signal processing

The above section has reviewed topics related to the role of ferrites in conventional microwave passive devices with emphasis placed on the circulator. This section covers three recent applications of low-loss ferrite films for high-frequency signal processing applications. The topics reviewed here concern spin wave parametric pumping and nonlinear spin waves in feedback rings. The specific work was done with single crystal YIG thin films due to their ultra low microwave loss properties. Similar devices can be realized using other categories of low-loss ferrites.

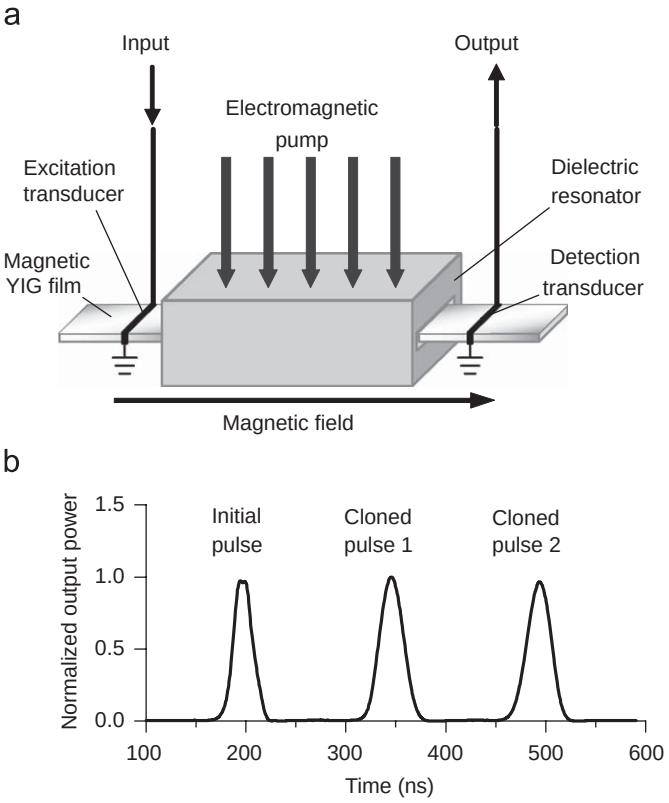

Fig. 8. (a) Schematic set up for spin wave pulse cloning experiments. (b) Representative output signals.

3.2.1. Cloning

The use of YIG films and parametric pumping techniques to clone spin wave pulses have been demonstrated recently [124]. Fig. 8(a) shows the basic arrangement. One starts with a YIG film strip with two transducers for the excitation and detection of spin waves. The film strip is placed inside an open dielectric resonator. The part of the film strip inside the resonator comprises the pumping region. A rectangular waveguide is used to deliver the pump power to the resonator. The cloning process occurs as follows. (1) A signal pulse at some carrier frequency, ω_s, is applied to the excitation transducer. (2) This signal produces a spin wave pulse in the film strip that travels toward the detection transducer. (3) Just before the spin wave pulse exits the pumping region, a pumping pulse with a carrier frequency at $\omega_p = 2\omega_s$ is applied to the resonator. (4) The parametric interaction between the spin wave pulse and the pumping pulse amplifies the forward traveling spin wave pulse and creates a new reversed spin wave pulse as well that travels back toward the excitation transducer. (5) Right before the new reversed pulse exits the pumping region, a second pumping pulse is applied to the resonator. (6) The parametric process repeats and another new reversed spin wave pulse is produced that travels toward the detection transducer. This second reversed pulse is actually a clone of the initial spin wave pulse. One can use more pumping pulses to produce

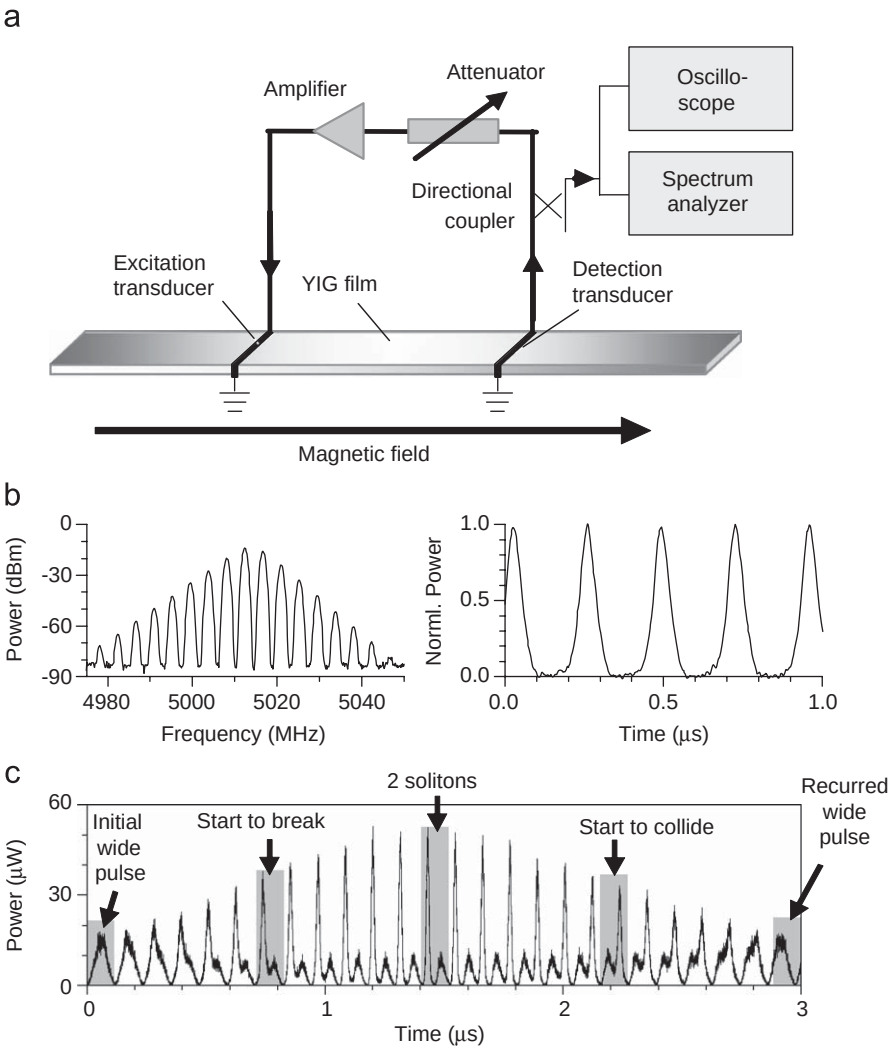

Fig. 9. (a) Schematic of the magnetic film feedback ring system. (b) Representative signals for soliton self-generation. (c) Representative signals for Fermi–Pasta–Ulam recurrence.

additional clones. Fig. 8(b) shows an output signal obtained under the application of properly timed four pumping pulses [124].

3.2.2. Feedback rings

In recent years, ferrite film-based active feedback rings have shown great promise for high-frequency applications [125–128]. Fig. 9(a) shows a typical YIG film strip feedback ring arrangement. The output signal from the detection transducer is fed back to the excitation transducer through an adjustable microwave attenuator and a microwave amplifier. This ring system can have a number of resonance eigenmodes that exhibit low decay rates [126]. For low values of the ring gain, all of the eigenmodes experience an overall net loss and there is no spontaneous signal in the ring. If the ring gain is increased to a certain threshold level, the eigenmode with the lowest decay rate will start to self-generate and one will obtain a continuous wave response at this eigenmode frequency. A further increase in the ring gain results in the generation of additional modes through a four-wave process. In the time domain, this corresponds to the formation of a spin wave pulse that circulates in the ring. The power of the circulating spin wave pulse increases with the ring gain. At some secondary gain threshold, at which the nonlinearity-induced pulse narrowing is strong enough to balance the dispersion-induced pulse broadening, the pulse evolves into an envelope soliton. Fig. 9(b) shows representative signals for such a soliton self-generation regime.

3.2.3. Fermi–Pasta–Ulam (FPU) recurrence

With a further increase in the ring gain, the pulse power becomes too high to maintain a single soliton state and the pulse breaks up into two separated solitons with different speeds. The slow overtake and subsequent collision of these two solitons leads to the reconstruction of the initial single pulse, namely, a recurrence of the initial state. Such a recurrence is called a Fermi–Pasta–Ulam recurrence. This effect was demonstrated recently with the same feedback ring configuration as in Fig. 9(a). Fig. 9(c) shows full cycle of pulse responses that show FPU recurrence. These data were obtained at a ring gain of 0.6 dB higher than the self-generation threshold.

The above-reviewed phenomena or techniques have high potential for microwave signal processing applications. The spin wave cloning technique can be used to develop a new type of microwave pulse multiplexers. The active feedback rings can work as a microwave or millimeter oscillator, a phase-locked frequency comb generator, or a microwave short pulse oscillator [127]. The phenomenon of FPU recurrences in feedback rings may lead to a new scheme for secure communications [128].

The above results represent only a small part of the progress in recent years in the use of ferrite films for high-frequency signal processing. Nevertheless, they demonstrate that the ferrite films have high potential for signal processing applications in radar and communication systems, among others. In terms of future developments, it is expected that these and similar device structures will make use of low-loss high anisotropy hexagonal ferrite thin films for the blossoming field of millimeter wave ferrite devices. It is also anticipated that new classes of multi-functional magneto-electric thin film materials and heterostructures, as in Ref. [129], will lead to new capabilities that involve the low-power electric field tuning of these and similar high-frequency magnetic devices.

3.3. Electromagnetic interference (EMI) suppressors

Traditionally, ferrite beads have been extensively used in the industry to suppress unwanted high-frequency electromagnetic noise. The driving idea for these noise suppressors is the mediation of the rf magnetic field, which is generally a maximum near the conductor, by the placement of a material that has large magnetic losses in close proximity. The key properties regarding this application are permeability losses, $\mu''(\omega)$, at high frequencies $f=\omega/2\pi$. Sintered ferrite beads are convenient when dealing with wires, but when dealing with noise suppression in printed and integrated circuits, planar materials or sheets that can be easily cut to the shape of the radiating component are needed. Composites based on oriented ferromagnetic flakes within an insulating matrix have been developed for that purpose. But, it has also been found that non-sintered ferrite films could be produced with excellent permeability levels at elevated frequencies [130]. In a first approach, the efficiency of the noise suppression is proportional to the real part impedance of the magnetic materials placed near the conductor. The inductance depends on the geometry, and is proportional to the magnetic permeability of the noise suppressor. As a consequence, the quantity $\omega\times\mu''(\omega)$ is a relevant figure of merit for EMI suppressors. It has been shown that the integral of this quantity over the whole spectrum is proportional to the square of the saturation magnetization [131]. Hexagonal ferrites may achieve higher figure of merits. In the previous section, we discussed recent advances in ferrite materials processing methodologies, notably spin spray ferrite plating, that now allow for the coating of IC components with ferrite films and coatings fabricated in a low-temperature process. This is a significant advance in our ability to eliminate or significantly reduce EMI by the use of ferrite coatings.

3.4. Ferrite-based tunable negative index metamaterials in microwave electronics

Recent advances in metamaterials possessing negative index of refraction (NIM) and strong dispersion characteristics with high values of $dn/d\omega$ ($\theta=n\omega\Delta L/c$) (TEM mode wave propagation assumed) has enabled a new generation of novel microwave technologies. Here n is the index of refraction, θ is the phase change of the signal through the material, ΔL is the length of the material and c is the velocity of light. A significant recent development in the field of NIMs is the fabrication of tunable negative index materials (TNIMs) utilizing high-quality ferrite materials [132–135]. The tunability and low losses observed in the NIM make them ideal materials for designing tunable, compact, and light weight phase shifters (among other devices).

Phase shifters are critical elements in several electronically tuned microwave systems in defense, space, and commercial communication applications. Excessive cost and weight of the phase shifters have limited the deployment of electronically scanned antennas in some aero-space applications. While digital diode based phase shifters may withstand high power of the order of a few tens of watts, by virtue of their nature, the accuracy in phase shift is limited. Hence, there is significant demand in the microwave industry for affordable, light weight, and high-power phase shifters. Microwave ferrite phase shifters can generally handle higher power than competing technologies. For example, commercial ferrite phase shifters can operate at an average power of up to 100 W and a peak power up to 2000 W. In ferrite phase shifters, a change in permeability by the application of magnetic field causes a change in the phase velocity of the microwave signal traveling through the phase shifter.

Traditional ferrite phase shifters operate at frequencies far from the FMR in order to avoid absorption losses near the FMR frequency. As a result, the real part of the complex permeability, μ', is necessarily small as illustrated in Fig. 10(a). It was previously reported both experimental and theoretical investigations of field tunable negative refractive index metamaterial (TNIM) using yttrium iron garnet films and an array of copper wires in waveguides that demonstrated a key feature of magnetic field tunability of the NIM in the microwave frequency region [132–135]. Transmission passbands were realized in the negative

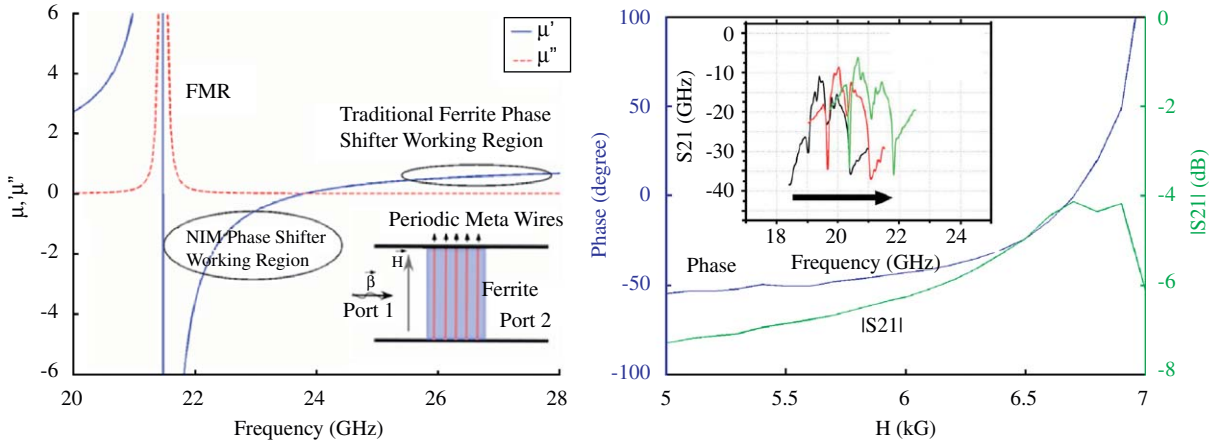

Fig. 10. (a) The effective permeability of a ferrite film near FMR illustrating the working frequency regions of both traditional ferrite phase shifter and NIM phase shifter. And the inset shows the schematic plot of a tunable NIM composite in a transmission line. The ferrite films are positioned together with periodic metal wires and a bias field was applied, $\vec{H}$. (b) The measured insertion phase shift and insertion loss (|S21|) vs. external magnetic field at 24 GHz. The inset demonstrates the magnetic field tuning of the NIM pass band. And the arrow indicates the direction that the pass band moves on when increasing the field.

refractive index region that could be tuned by an external magnetic field. The permeability of the NIM was simultaneously tuned along with refractive index. The change in permeability or refractive index leads to a change in the phase velocity of the signal and, therefore, the phase of the transmission coefficient.

The advantage of using a ferrite NIM material for phase shifter applications is that it allows the use of a ferrite in the negative μ' region near the FMR when μ' is relatively high and still maintains low losses [135]. Near the FMR frequency, the magnitude ofμ' is larger than that at frequencies away from it. Assuming the loss factor to be about the same for the NIM and the conventional ferrite phase shifter, we would expect a much improved figure of merit using the NIM composite, since the phase shifts would be significantly higher due to higher differentialμ' as illustrated in Fig. 10a. In the field tunable NIM, the effect of the YIG film was to provide a tunable negative permeability over a continuous range of frequencies on the high-frequency side of the FMR. Complementary negative permittivity, ε', is achieved using a single periodic array of copper thin film wires deposited on a Kapton^{TM} substrate. The inset of Fig. 10a shows a schematic diagram of the side view of a tunable NIM in a transmission line. The composite structure consisted of periodic thin metal wires and high-quality ferrite films. In the work of He et al. [135], a negative refractive index region of 0.5 GHz width in K-band was determined from measurements. Although theoretically YIG has a negative μ' region with a band width of up to 2.5 GHz, the small negative refractive index region was due to the small volume factor of the YIG slabs. However, increasing the volume of the YIG will increase the absorption. Therefore, there is a tradeoff between wide band width for negative index region and low loss. In addition, the dielectric permittivity of the YIG slabs reduces the effective negative permittivity obtained from the plasmonic copper wires.

The phase shift of a 1 cm long sample NIM composite, as well as the insertion loss performance of the 8 mm long sample, are shown in Fig. 10b. The inset illustrates the field tuning of the passband corresponding NIM region. At 24 GHz, when the applied magnetic field was varied from 6.0 to 7.0 kOe, the phase varied 160° with the insertion loss varying from 4.3 to 6.3 dB. At the lower field side, the phase change was smaller. The phase shifter was operated at the frequency above the ferromagnetic anti-resonance with a positive permeability with the material having a positive refractive index. At higher fields, the phase was more sensitive to field tuning and the insertion loss was even smaller, which corresponded to the negative refractive index region as illustrated in Fig. 10a. Overall, the insertion loss had a variation of 2 dB, as a result of variation in wave impedance due to changes in the permeability. In summary, it has been demonstrated a waveguide field tunable phase shifter using a ferrite-based NIM composite. Continuous and rapid phase tunability of 160°/kOe was realized with an insertion loss of 4–7 dB at 24 GHz. Recently, these studies have been extended to realize the first microstrip TNIM-based phase shifter [139]. The co-development of multiferroic transducer heterostructures will allow for electric field tunability of phase shifters and other microwave EM devices [140,141].

4. Outlook

Ferrite materials have been studied since the 1930s and their application in microwave device technology dates to the 1950s. For this reason ferrites are considered a mature technology with the implication being that anticipated advances will be incremental. This, in fact, is far from reality. Advances in materials processing and devices taking place during the last 10 years have been dramatic and significant.

Alternating target laser ablation deposition has been shown to allow the manipulation of cations within a unit cell providing opportunities to fabricate far from equilibrium structures and ultimately to tailor magnetic, electronic, and microwave properties for specific applications. Screen printing has been shown to be an effective tool in the processing of thick, self-biased, and low-loss ferrite films. These breakthroughs could prove to be disruptive advances in monolithic microwave-integrated circuits technology. Still, when nothing less than single crystal quality, low-loss ferrites are needed, LPE and QSC compacts provide thick films with low FMR linewidths. Further work is needed to optimize the growth of Li-ferrites using these techniques to address the needs of low-frequency device applications (e.g. C-, S-, and X-bands).

In addition to material advances, we find that new devices having enhanced performance, reduced size, and in some instances added functionality, have been realized. The ability to process thick film ferrites having perpendicular magnetic anisotropy and self-bias properties allows for the redesign of conventional microwave passives as light weight planar constructs. Likewise, low-temperature processing of ferrite coatings on plastics allow for a wide range of improved EMI suppression. New devices based upon spin wave parametric pumping and nonlinear spin waves in feedback rings employ ferrite films for high-frequency signal processing. Finally, NIM constructs employing low-loss ferrites, allow for a new class of tunable microwave electronics that are small in size, profile, and weight. The co-development of multiferroic transducer substrates will allow for electric field tunable microwave electronics giving rise to such enhanced performance as dynamic band widths and voltage turned phase shifting.

In lieu of these advances, it appears that the microwave materials and device technologies are in a state of significant positive change with the potential to greatly impact a wide range of technologies that involve the sending, receiving, and manipulation of electromagnetic signals.

References

[1] G.P. Rodrigue, Proc. IEEE 76 (1988) 121;
E.F. Schloemann, J. Magn. Magn. Mater. 209 (2000) 15;
J.D. Adam, L.E. Davis, G.F. Dionne, E.F. Schloemann, S.N. Stitzer, IEEE Trans. Microwave Theory Tech. 50 (2002) 721.
[2] H.A. Kramers, Physica 1 (1999) 182;
L. Néel, Ann. Phys. (Paris) 3 (1948) 137;
P.W. Anderson, Phys. Rev. 79 (1950) 350;
J.H. van Vleck, J. Phys. Rad. 12 (1951) 1178;
E.W. Gorter, Proc. IRE 104B (1957) 255;
J.B. Goodenough, J. Phys. Chem. Solids 6 (1958) 287;
P.W. Anderson, Phys. Rev. 79 (1959) 115;
J. Kanamori, J. Phys. Chem. Solids 10 (1959) 67.
[3] R.C. Lecraw, E.G. Spencer, C.S. Porter, Phys. Rev. 110 (1958) 1311–1313.
[4] J.J. Went, G.W. Rathenau, E.W. Gorter, et al., Philips Tech. Rev. 13 (1951) 194;
J. Smit, H.G. Beljers, Philips Res. Rep. 10 (1955) 113.
[5] J. Smit, H.P.J. Wijn, Ferrites, Wiley, New York, 1959, pp. 191–211.
[6] T.M. Perekalina, V.P. Cheparin, Fiz. Tverd. Tela 9 (1967) 217;
T.M. Perekalina, M.A. Vinnik, R.I. Zevereva, et al., Zh. Eksp. Teor. Fiz. 59 (1970) 1490;
G. Albanese, A. Deriu, Ceramargia Int. 5 (1979) 3.
[7] L.G. Van Uitert, F.W. Swanekamp, J. Appl. Phys. 28 (1957) 482;
A.H. Mones, E. Banks, J. Phys. Chem. Solids 4 (1958) 217;
K. Haneda, H. Kojima, Jpn. J. Appl. Phys. 12 (1973) 355.
[8] P.C. Dorsey, S.E. Bushnell, R.G. Seed, et al., J. Appl. Phys. 74 (1993) 1242.
[9] P.C. Dorsey, S.E. Bushnell, R.G. Seed, et al., IEEE Trans. Mag. 29 (1993) 3069.
[10] B.M. Simion, R. Ramesh, V.G. Keramidas, et al., J. Appl. Phys. 76 (1994) 6287.
[11] B.M. Simion, G. Thomas, R. Ramesh, et al., Appl. Phys. Lett. 66 (1995) 830.
[12] H. Buhay, J.D. Adam, M.R. Daniel, et al., IEEE Trans. Mag. 31 (1995) 3832.
[13] Y. Nakata, Y. Tashiro, T. Okada, et al., Proc. SPIE 4088 (2000) 333.
[14] S. Higuchi, K. Ueda, F. Yahiro, et al., IEEE Trans. Mag. 37 (2001) 2451.
[15] H. Hayashi, S. Iwasa, N.J. Vasa, et al., Jpn. J. Appl. Phys. 41 (2002) 410.
[16] H. Hayashi, S. Iwasa, N.J. Vasa, et al., Appl. Surf. Sci. 197 (2002) 463.
[17] M.Y. Chern, W.S. Lee, D.R. Liou, J. Magn. Magn. Mater. 170 (1997) L243.
[18] C. Vittoria, U.S. Patent No. 5,227,204, 1993 (disclosed 1991).

[19] P.R. Dorsey, C. Seed, C. Vittoria, et al., IEEE Trans. Magn. 28 (1992) 3216.
[20] Y. Song, S. Kalarickal, C.E. Patton, J. Appl. Phys. 94 (2003) 5103.
[21] R. Welch, T. Jackson, S. Palmer, IEEE Tran. Magn. 31 (1995) 2752.
[22] S.D. Yoon, C. Vittoria, S.A. Oliver, J. Magn. Magn. Mater. 265 (2003) 130.
[23] X.H. Liu, M.H. Hong, W.D. Song, et al., Appl. Phys. A 80 (2005) 611.
[24] Z.H. Chen, A. Yang, S.D. Yoon, et al., J. Magn. Magn. Mater. 301 (2006) 166.
[25] Z.H. Chen, A. Yang, Z.H. Cai, et al., IEEE Trans. Magn. 42 (2006) 2855.
[26] M. Koleva, S. Zotova, P. Atanasov, et al., Appl. Surf. Sci. 168 (2000) 108.
[27] J.C. Faloh-Gandarilla, S. Diaz-Castanon, F. Leccabue, et al., J. Alloys Compd. 369 (2004) 195.
[28] S. Oliver, M. Chen, C. Vittoria, et al., J. Appl. Phys. 85 (1999) 4630.
[29] R. Atkinson, P. Papakonstantinou, I. Salter, et al., J. Magn. Magn. Mater. 138 (1994) 222.
[30] O. Heczko, R. Gerber, Z. Simsa, Thin Solid Films 358 (2000) 206.
[31] K. Tanaka, Y. Omata, Y. Nishikawa, et al., IEEE Trans. J. Magn. Japan 6 (1991) 1001.
[32] M.T. Johnson, P.G. Kotula, C.B. Carter, J. Cryst. Growth 206 (1999) 299.
[33] C.N. Chinnasamy, S.D. Yoon, A. Yang, et al., J. Appl. Phys. 101 (2007) 09M517.
[34] G. Balestrino, S. Martellucci, A. Paoletti, et al., Solid State Commun. 96 (1995) 997.
[35] J. Cillessen, R. Wolf, J. Giesbers, et al., Appl. Surf. Sci. 96 (1996) 744.
[36] M. Guyot, A. Lisfi, R. Krishnan, et al., Appl. Surf. Sci. 96–98 (1996) 802.
[37] A. Yang, Z. Chen, X. Zuo, et al., Appl. Phys. Lett. 86 (2005) 252510.
[38] X. Zuo, A. Yang, S.D. Yoon, et al., Appl. Phys. Lett. 87 (2005) 152505.
[39] A. Yang, Z. Chen, S.M. Islam, C. Vittoria, V.G. Harris, J. Appl. Phys. 103 (2008) 07E509.
[40] X. Zuo, A. Yang, C. Vittoria, et al., J. Appl. Phys. 99 (2006) 08M909.
[41] M. Abe, Y. Tamaura, J. Appl. Phys. 55 (1984) 2614;
M. Abe, Y. Tamaura, Y. Goto, N. Kitamura, M. Gomi, J. Appl. Phys. 61 (1987) 3211.
[42] K. Kondo, Y. Numata, T. Chiba, S. Yamada, S. Yoshida, Y. Shimada, N. Matsishita, M. Abe, Trans. Magn. Soc. Japan 5 (2005) 161.
[43] M. Abe, T. Itoh, Y. Tamaura, Y. Gotoh, M. Gomi, IEEE Trans. Magn. 23 (1987) 3736.
[44] K. Kondo, T. Chiba, H. Ono, S. Yoshida, Y. Shimada, N. Matsishita, M. Abe, in: Proceedings of the Ninth International Conference on Ferrites (ICF-9), San Francisco, 2004, pp. 659–663.
[45] K. Kondo, T. Chiba, H. Ono, S. Yoshida, Y. Shimada, N. Matsishita, M. Abe, J. Appl. Phys. 93 (2003) 7130.
[46] N. Matsishita, K. Kondo, S. Yoshida, M. Tada, M. Yoshimura, M. Abe, J. Electroceram. 16 (2006) 557.
[47] K. Kondo, S. Yoshida, H. Ono, M. Abe, J. Appl. Phys. 101 (2007) 09M502.
[48] R.C. Linares, J. Cryst. Growth 3 (1968) 443.
[49] T. Hibiya, J. Cryst. Growth 62 (1983) 87.
[50] P. Hansen, K. Witter, W. Tolksdorf, Phys. Rev. B 27 (1983) 6608.
[51] T. Sekijima, T. Fujii, K. Wakino, et al., IEEE MTT-S Dig. (1999) 1369.
[52] G.F. Dionne, J.A.S. Weiss, G.A. Allen, et al., IEEE MTT-S Dig. (1988) 127.
[53] M.R. Webb, Int. J. Infrared Millimeter Waves 10 (1989) 1317.
[54] H.L. Glass, Proc. IEEE 76 (1988) 151.
[55] J.M. Robertson, M. Jansen, B. Hoekstra, et al., J. Cryst. Growth 41 (1977) 29.
[56] P.J.M. van der Straten, R. Metselaar, IEEE Trans. Magn. 14 (1978) 421.
[57] J.M. Robertson, J.P.M. Damen, H.A. Algra, IEEE Trans. Magn. 15 (1979) 1870.
[58] H.L. Glass, F.S. Stearns, L.R. Adkins, in: Proceedings of the Third ICF, Kyoto, Japan, 1980, p. 39.
[59] P.J.M. van der Straten, R. Metselaar, J. Cryst. Growth 14 (1980) 114.
[60] F.S. Stearns, H.L. Glass, Mater. Res. Bull. 11 (1976) 1319.
[61] H.L. Glass, F.S. Stearns, IEEE Trans. Magn. 13 (1977) 1241.
[62] H.L. Glass, J.H.W. Liaw, J. Appl. Phys. 49 (1978) 1578.
[63] F. Haberey, R. Leckebusch, M. Rosenberg, K. Sahl, Mater. Res. Bull. 15 (1980) 493.
[64] H. Dotsch, D. Mateika, P. Roschmann, W. Tolksdorf, Mater. Res. Bull. 18 (1983) 1209.
[65] W.E. Kramer, A.M. Stewart, R.H. Hopkins, et al., IEEE Trans. Magn. 22 (1986) 981.
[66] H. Dotsch, D. Mateika, P. Roschmann, W. Tolksdorf, Mater. Res. Bull. 18 (1983) 1209.
[67] M. Mita, J. Phys. Soc. Japan 18 (1962) 155.
[68] F.R. Morgenthaler, Proc. IRE 50 (1962) 2139.
[69] M. Labeyrie, J.C. Mage, W. Simonet, et al., IEEE Trans. Magn. 20 (1984) 1224.
[70] L.M. Silber, W.D. Wilber, IEEE Trans. Magn. 22 (1986) 984.
[71] M.S. Yuan, H.L. Glass, L.R. Adkins, Appl. Phys. Lett. 53 (1988) 340.
[72] S.G. Wang, S.D. Yoon, C. Vittoria, J. Appl. Phys. 92 (2002) 3283.
[73] S.D. Yoon, C. Vittoria, J. Appl. Phys. 93 (2003) 8597.
[74] S.D. Yoon, C. Vittoria, IEEE Trans. Magn. 39 (2003) 3163.
[75] S.D. Yoon, C. Vittoria, J. Appl. Phys. 96 (2004) 2131.
[76] J. Topfer, J. Mürbe, A. Angermann, S. Kracunovska, S. Barth, F. Bechtold, Int. J. Appl. Ceram. Technol. 3 (2006) 455.
[77] K.I. Arshak, A. Ajina, D. Egan, Microelectron. J. 32 (2001) 113.
[78] N.J. Grabham, S.P. Beeby, N.M. White, Sensors Actuators A 110 (2004) 365.
[79] V.G. Harris, Z. Chen, Y. Chen, S. Yoon, T. Sakai, A. Gieler, A. Yang, Y. He, K.S. Ziemer, N.X. Sun, C. Vittoria, J. Appl. Phys. 99 (2006) 08M911.
[80] Z.C. Yuan, A.J. Williams, T.C. Shields, S. Blackburn, C.B. Ponton, J. Magn. Magn. Mater. 247 (2002) 257.
[81] Y. Chen, A.L. Geiler, T. Sakai, S.D. Yoon, C. Vittoria, V.G. Harris, J. Appl. Phys. 99 (2006) 08M904.
[82] Y. Chen, T. Sakai, T. Chen, S.D. Yoon, C. Vittoria, V.G. Harris, J. Appl. Phys. 100 (2006) 043907.
[83] Y. Chen, T. Sakai, T. Chen, S.D. Yoon, A.L. Geiler, C. Vittoria, V.G. Harris, Appl. Phys. Lett. 88 (2006) 062516.
[84] V.G. Harris, C. Vittoria, F. Rachford, Y. Chen, U.S. Patent Pending, 2008 (disclosed 2007).
[85] T. Sakai, Y. Chen, C.N. Chinnasamy, C. Vittoria, V.G. Harris, IEEE Trans. Magn. 42 (2006) 3353.
[86] Yajie Chen, Michael J. Nedoroscik, Anton L. Geiler, Carmine Vittoria, Vincent G. Harris, Perpendicularly oriented polycrystalline BaFe11.1Sc0.9O19 hexaferrite with narrow FMR linewidth, J. Am. Ceram. Soc. 91 (2008) 2952–2956.
[87] Y. Chen, A.L. Geiler, T. Chen, T. Sakai, C. Vittoria, V.G. Harris, J. Appl. Phys. 101 (2007) 09M501.
[88] J.L. Snoek, Physics 3 (1936) 463.
[89] J.L. Snoek, Philips Tech. Rev. 8 (1946) 353.
[90] G.P. Rodrigue, Proc. IEEE 76 (1988) 121.
[91] B. Lax, Proc. IRE 44 (1956) 1368.
[92] F. Bertaut, F. Forrat, Compt. Rend. 242 (1956) 382.
[93] F. Bertaut, R. Pauthenet, Proc. Inst. Elec. Eng. 104B (1957) 261.
[94] J.F. Dillon, Phys. Rev. 105 (1957) 759.
[95] D.J. DeBitetto, F.K. DePre, F.G. Brockman, in: Proceedings of the Symposium on Millimeter Waves, vol. 9, 1959, p. 95.
[96] E.F. Schloemann, Proc. IEEE 76 (1988) 188.
[97] A.J. Fenn, D.H. Temme, W.P. Delaney, et al., Lincoln Lab. J. 12 (2000) 312.
[98] T. Schaug-Pettersen, ONR Tech. Rep. (BR) ONRL 111 (1957) 57.
[99] H.N. Chaitm, T.R. Curry, J. Appl. Phys. 30 (1959) 152S.
[100] L. Davis, J.U. Milano, J. Saunders, Proc. IRE 48 (1960) 115.
[101] B. Hershenov, In: IEEE-MTT 1967 Int. Microwave Symp. Dig., 1967, p. 142.
[102] H. Bosma, Proc. IEE 109 (1962) 137.
[103] H. Bosma, IRE Trans. Microwave Theory Tech. 12 (1964) 61.
[104] C.E. Fay, R.L. Comstock, IEEE Trans. Microwave Theory Tech. 13 (1965) 15.
[105] D. Polder, Philos. Mag. 40 (1949) 99.
[106] D. Polder, Phys. Rev. 73 (1948) 1120.
[107] Y.S. Wu, F.J. Rosenbaum, IEEE Trans. Microwave Theory Tech. 22 (1974) 849.
[108] R.H. Knerr, IEEE Trans. Microwave Theory Tech. 23 (1975) 818.
[109] W.H. Von Aulock, C.E. Fay, Linear Ferrite Devices for Microwave Applications, Academic Press, New York, 1968.
[110] J. Helszajn, Nonreciprocal Microwave Junctions and Circulators, Wiley, New York, 1975.
[111] C. Kittel, Phys. Rev. 73 (1948) 155.
[112] Y. Akaiwa, T. Okazaki, IEEE Trans. Microwave Theory Tech. 10 (1974) 374.
[113] J.A. Weiss, N.G. Watson, G.F. Dionne, IEEE MTT-S Dig. (1989) 145.
[114] N. Zeina, H. How, C. Vittoria, IEEE Trans. Magn. 28 (1992) 3219.
[115] S.A. Oliver, P. Shi, W. Hu, et al., IEEE Trans. Microwave Theory Tech. 49 (2001) 385.
[116] P. Shi, H. How, Xu. Zuo, et al., IEEE Trans. Magn. 37 (2001) 2389.
[117] L.E. Davis, D. Sillars, IEEE Trans. Microwave Theory Tech. 34 (1986) 804.
[118] D. Marcuse, Bell Syst. Tech. J. 54 (1975) 985.
[119] I. Awai, T. Itoh, IEEE Trans. Microwave Theory Tech. 29 (1981) 1077.
[120] J. Mazur, M. Mrozowski, IEEE Trans. Microwave Theory Tech. 37 (1989) 159.
[121] C.K. Queck, L.E. Davis, IEEE Trans. Microwave Theory Tech. 50 (2002) 2910.
[122] S.D. Yoon, J.W. Wang, N.X. Sun, et al., IEEE Trans. Magn. 43 (2007) 2639.
[123] C.K. Queck, L.E. Davis, Electron. Lett. 39 (2003) 1595.
[124] K.R. Smith, V.I. Vasyuchka, M. Wu, G.A. Melkov, C.E. Patton, Phys. Rev. B 76 (2007) 054412.
[125] B.A. Kalinikos, M.M. Scott, C.E. Patton, Phys. Rev. Lett. 84 (2000) 4697.
[126] M. Wu, B.A. Kalinikos, C.E. Patton, Phys. Rev. Lett. 95 (2005) 237202.
[127] M. Wu, B.A. Kalinikos, L.D. Carr, C.E. Patton, Phys. Rev. Lett. 96 (2006) 187202.
[128] M. Wu, C.E. Patton, Phys. Rev. Lett. 98 (2007) 047202.
[129] J. Das, B.A. Kalinikos, A.R. Barman, C.E. Patton, Appl. Phys. Lett. 91 (2007) 172516.
[130] O. Acher, M. Ledieu, M. Abe, M. Tada, N. Matsushita, M. Yoshimura, K. Kondo, J. Magn. Magn. Mater. 310 (2007) 2532.
[131] O. Acher, A.L. Adenot, Phys. Rev. B 62 (2000) 11324.
[132] Y. He, P. He, S.D. Yoon, P.V. Parimi, F.J. Rachford, V.G. Harris, C. Vittoria, J. Magn. Magn. Mater. 313 (2007) 187.
[133] H. Zhao, J. Zhou, Q. Zhao, B. Li, L. Kang, Appl. Phys. Lett. 91 (2007) 131107.
[134] Y. He, P. He, V.G. Harris, C. Vittoria, IEEE Trans. Magn. 42 (2006).
[135] P. He, P. Parimi, V.G. Harris, C. Vittoria, Electron. Lett. 43 (2007) 1440.
[136] Z. Chen, et al., Epitaxial growth of M-type Ba-hexaferrite films on MgO (1 1 1) SiC (0 0 0 1) with low ferromagnetic resonance linewidths, Appl. Phys. Lett. 91 (2007) 182505.
[137] Aria Yang, Zhaohui Chen, Anton Geiler, Xu Zuo, Daniel Haskel, E. Kravtsov, C. Vittoria, V.G. Harris, Element and site-specific oxidization state and cation distribution in manganese ferrite films by diffraction anomalous fine structure, Appl. Phys. Lett. 93 (2008) 052504.
[138] Anton L. Geiler, Aria Yang, Xu Zuo, Soack Dae Yoon, Yajie Chen, Vincent G. Harris, Carmine Vittoria, Atomic scale design and control of cation distribution in hexagonal ferrites, Phys. Rev. Lett. 101 (2008) 067201.
[139] P. He, J. Gao, C. Marinis, P.V. Parimi, V.G. Harris, C. Vittoria, Microstrip Negative Refractive Index Metamaterial and Phase Shifter, Appl. Phys. Lett. 93 (2008) 193505.
[140] J. Zhai, Z. Xing, S. Dong, J. Li, D. Viehland, J. Am. Ceram. Soc. 91 (2008) 351.
[141] M.I. Bichurin, D. Viehland, G. Srinivasan, J Electroceram 19 (2007) 1385.